Mineralogical Magazine, October 2010, Vol. 74(5), pp. 849–857

The electrical conductivity of dry polycrystalline olivine compacts at high temperatures and pressures

LIDONG DAI[1], HEPING LI[1,*], CHUNHAI LI[2], HAIYING HU[1,3] AND SHUANGMING SHAN[1]

[1] Laboratory for Study of the Earth's Interior and Geofluids, Institute of Geochemistry, Chinese Academy of Sciences, Guiyang, Guizhou 550002, China
[2] State Key Laboratory for Mineral Deposits Research, Nanjing University, Nanjing, Jiangsu 210093, China
[3] Graduate School of the Chinese Academy of Sciences, Beijing 100039, China

[*Received 21 May 2010; Accepted 1 September 2010*]

ABSTRACT

The electrical conductivity of dry polycrystalline olivine compacts (hot-pressed and sintered pellets) was measured at pressures of 1.0–4.0 GPa, at temperatures of 1073–1423 K, and at different oxygen fugacities *via* the use of a YJ-3000t multi-anvil press. Oxygen fugacity was controlled successfully by means of five solid buffers: Fe_3O_4-Fe_2O_3, Ni-NiO, Fe-Fe_3O_4, Fe-FeO and Mo-MoO_2. Within the selected frequency range of 10^2–10^6 Hz, the experimental results indicate that the grain interior conduction mechanism is characterized by a semi-circular curve on an impedance diagram. As a function of increasing pressure, the electrical conductivity of polycrystalline olivine compacts decreases, whereas the activation enthalpy and the temperature-independent pre-exponential factors increase slightly. The activation energy and activation volume of polycrystalline olivine compacts were determined to be 141.02±2.53 kJ/mol and 0.25±0.05 cm^3/mol, respectively. At a pressure of 4.0 GPa, electrical conductivity was observed to increase as a function of increasing oxygen fugacity, and the relationship between electrical conductivity and oxygen fugacity can be described as $\log_{10}(\sigma) = (2.47\pm0.085) + (0.096\pm0.023) \times \log_{10} f_{O_2} + (-0.55\pm0.011)/T$, which presents the exponential factor q (~0.096). Our observations demonstrate that the primary conduction mechanism for polycrystalline olivine compacts is a small polaron.

KEYWORDS: electrical conductivity, polycrystalline olivine compacts, oxygen fugacity, high temperature, high pressure.

Introduction

ELECTRICAL conductivity and the elastic wave velocity of minerals and rocks at high temperatures and pressures are two crucial measurements that geophysicists use to explore the material characteristics of the deep Earth. Compared to elastic wave velocity, electrical conductivity is more sensitive to temperature. Therefore, the *in situ* measurement of the electrical conductivity of minerals and rocks at high pressures plays an important role in predicting the chemical composition and thermodynamic state of the interiors of the Earth and other planets (Omura *et al*., 1989; Zhang *et al*., 2006; Watson *et al*., 2010).

The electrical properties of minerals and rocks depend heavily on water content, chemical composition, grain boundary state, temperature, pressure, oxygen fugacity and frequency (Nover, 2005; Karato and Dai, 2009). Oxygen fugacity is a key parameter in constraining and adjusting the physical and chemical interaction processes within the crust, mantle, and core of the deep Earth where it plays a vital role in magma genesis, magma degassing, and metasomatic processes (Chou and Eugster, 1976; Chou, 1978; McCammon *et al*., 2004; Weston *et al*., 2009).

* E-mail: hepingli_2007@hotmail.com
DOI: 10.1180/minmag.2010.074.5.849

A variety of methods to control oxygen fugacity have been applied successfully to solid samples at high pressures (Frost, 1991; Yasuda and Fujii, 1993; Mendybaev *et al*., 1998; Dobson and Brodholt, 1999; Li *et al*., 1999). Recently, a new technique was designed and developed by the present authors to control oxygen fugacity through variations of solid oxygen buffer types. It is applicable to any large-volume, multi-anvil, high-pressure apparatus. We measured successfully the low-frequency, grain-boundary, electrical conductivity of dry synthetic peridotite, in addition to the electrical conductivity of hydrous wadsleyite (Dai *et al*., 2009*a*,*b*). This technique has been applied successfully to high-pressure measurements of low differential stress in olivine (Rubie *et al*., 1993), grain growth in hydrous wadsleyite (Nishihara *et al*., 2006), and hydrogen-related defect chemistry in hydrous wadsleyite (Nishihara *et al*., 2008). Oxygen fugacity along with temperature, pressure and water content control the electrical conductivity at high pressure.

A large body of evidence from geophysics, geochemistry, and petrology has established that the Earth's mantle consists primarily of peridotite, which contains 60 wt.% of normative olivine, 40 wt.% of normative pyroxene, and garnet (Ringwood, 1975, 1982; Irifune and Ringwood, 1987; Xu *et al*., 2000*a*; Ohta *et al*., 2010*a*). Thus, olivine and its polymorph phases of wadsleyite and ringwoodite, as dominant mineral phases, may control the electrical conductivity of the peridotite mantle from the bottom of the lower crust (~40 km) to the transition zone (410–660 km) (Xu *et al*., 1998, 2000*a*,*b*). The electrical conductivities of these representative minerals are the focus of current research. Hydrous olivine, orthopyroxene, garnet, wadsleyite and ringwoodite are the most prominent and abundant minerals in the depth range from the upper mantle to the transition zone (Xu *et al*., 1998; Huang *et al*., 2005; Wang *et al*., 2006; Romano *et al*., 2006, 2009; Karato, 2008*a*; Dai and Karato, 2009*b*,*c*,*d*; Zhang *et al*., 2010). Electrical conductivity data for dry polycrystalline olivine compacts under different oxygen fugacities have not yet been reported.

In the present experiment, at pressures of 1.0–4.0 GPa, temperatures of 1073–1423 K, and oxygen fugacity controlled by means of five solid buffers (Fe_3O_4-Fe_2O_3, Ni-NiO, Fe-Fe_3O_4, Fe-FeO and Mo-MoO_2), we used AC impedance spectra methods to conduct *in situ* measurements of the electrical conductivity of dry polycrystalline olivine compacts in the frequency range 10^2–10^6 Hz. A functional relationship between electrical conductivity and temperature, pressure and oxygen fugacity is established, and the conduction mechanism discussed.

Experimental procedures

All of the present experiments were conducted using a YJ-3000t instrument which is a large-volume, multi-anvil press, in combination with a Solarton-1260 impedance/gain-phase analyzer, in the Laboratory for Study of the Earth's Interior and Geofluids, Institute of Geochemistry, Chinese Academy of Sciences (CAS), China. This experimental device is similar to one used previously (Li *et al*., 1998; Xie *et al*., 2002). All microstructural observations, phase analyses, and water-content measurements, including micro-Raman spectrum and non-polarized transmission Fourier-transform infrared spectroscopy, were conducted at the Department of Geology and Geophysics, Yale University, USA. The dry polycrystalline olivine compacts were synthesized on a hot isostatic press at the Peking Iron & Steel Research Institute, China (see method in Dai *et al*., 2006). Electron probe analysis was performed at the State Key Lab of Ore Deposit Geochemistry, CAS, China. The chemical composition of these synthetic polycrystalline compacts is described in Table 1. Figure 1 depicts the experimental setup for the electrical conductivity measurements at high temperatures and high pressures. A detailed description of the experimental assembly was presented by Dai *et al*. (2008*b*). Here we focus on

TABLE 1. Chemical composition (wt.%) of dry polycrystalline olivine compacts.

Cr_2O_3	0.15
NiO	0.71
MnO	0.32
FeO	10.97
Na_2O	0.04
K_2O	0.18
Al_2O_3	0.23
CaO	0.16
MgO	45.79
TiO_2	0.20
SiO_2	41.24
Total	99.99

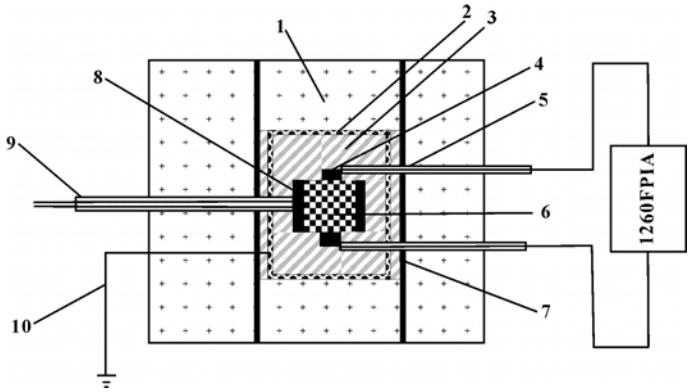

FIG. 1. Experimental setup for electrical conductivity measurements at high temperatures and pressures: (1) pyrophyllite (sintered at 973 K); (2) metal shielding cases (made of Ni, Fe or Mo); (3) insulating alumina; (4) buffering electrode; (5) nickel-lead insulating sleeve; (6) sample; (7) stainless-steel heater; (8) solid buffer tube; (9) Pt-$PtRh_{10}$ thermocouple and insulating sleeve; (10) earth line.

the experimental principles of controlling oxygen fugacity.

An entire series of metals and their corresponding metal oxides were selected to control and adjust oxygen fugacity. Several different mixtures of metals and metal oxides were pressed and sintered using a hot isostatic press. An electric sparking discharge erosion technique was used to cut and polish materials into regular metal buffer sleeves and buffer electrodes. We successfully established and developed this oxygen buffering technique by varying the types of metal in the metal sleeves and in the corresponding electrodes of the large-volume, high-pressure multi-anvil apparatus, such as the YJ-3000t and the Kawai-1000t (Rubie *et al*., 1993; Nishihara *et al*., 2006, 2008; Dai *et al*., 2009*a*; Campbell *et al*., 2009). Under the aforementioned *P-T* conditions, the oxygen fugacity buffer reached a thermodynamic balance according to the following equation:

$$MO_{\gamma} + \gamma/2\, O_2 \rightleftharpoons MO_{(\lambda+\gamma)} \quad (1)$$

where *M* represents Ni, Fe and Mo; λ represents a value of 0 or 4/3; and γ represents a constant that depends on the valence state of *M*. At constant *P-T*, the experimental conditions have reached an exact physical and chemical balance when the impedance reaches a constant value. The metal-oxygen buffers are proven to be feasible and effective if the X-ray diffraction (XRD) results of the two original phases of the recovery buffers coexist for the metal and corresponding metal oxide. When reaction 1 reaches chemical equilibrium, the oxygen fugacity value of each oxygen buffer can be described as a function of both temperature and pressure as follows:

$$f_{O_2} = B^{2/\gamma} \exp\left\{\frac{2P(V_{MO_{(\lambda+\gamma)}} - V_{MO_{(\lambda)}})}{\gamma RT}\right\} \quad (2)$$

where B is the balance constant at an ambient pressure that depends on the temperature, and $V_{MO_{(\lambda+\gamma)}}$ and $V_{MO_{\lambda}}$ represent the molar volumes of the solid oxygen buffering pairs. According to this formula, we can calculate the oxygen fugacity value that corresponds to each solid buffer at different temperatures under the conditions of 4.0 GPa, as shown in Fig. 2. The buffers in the order from the most oxidizing to the most reducing are as follows: Fe_3O_4-Fe_2O_3, Ni-NiO, Fe-Fe_3O_4, Fe-FeO and Mo-MoO_2.

Results

In situ measurements of the electrical conductivity of dry polycrystalline olivine compacts were carried out at a pressure of 1.0−4.0 GPa, temperature of 1073−1423 K and an oxygen partial pressure controlled by means of an Mo-MoO_2 oxygen buffer. The same measurements were made under the same *P-T* conditions for an oxygen partial pressure controlled by means of five oxygen buffers (Fe_3O_4-Fe_2O_3, Ni-NiO, Fe-Fe_3O_4, Fe-FeO, and Mo-MoO_2). The frequency range and the signal voltage were 10^2−10^6 Hz and 1.0 V, respectively.

Representative impedance spectra under the conditions of 4.0 GPa, 1073−1423 K, and an

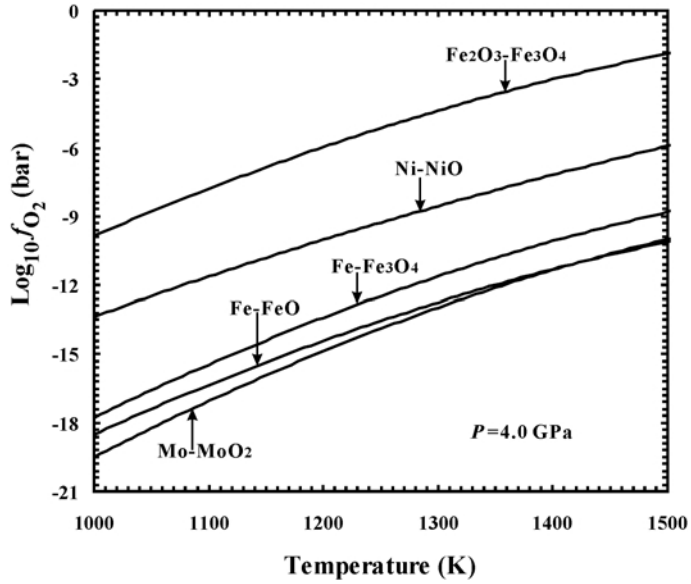

FIG. 2. The dependence of the logarithm of oxygen fugacity, f_{O_2}, on the temperature at P = 4.0 GPa for the Fe_3O_4-Fe_2O_3, Ni-NiO, Fe-Fe_3O_4, Fe-FeO, and Mo-MoO_2 solid buffers. Each oxygen fugacity value at high temperature and pressure was obtained from equation 2.

oxygen partial pressure controlled *via* Mo-MoO_2 are depicted in Fig. 3. The results obtained under different oxygen partial pressure conditions are similar to those illustrated in Fig. 3. On the basis of impedance spectra theory (Tyburczy and Roberts, 1990; Roberts and Duba, 1995; Bagdassarov and Schmeling, 2005), the complex impedance of polycrystalline olivine compacts is the total opposition for a given AC signal, which is described by a real component (Z'), an imaginary component (Z), a magnitude ($|Z|$), a phase angle (Φ), a resistance (R), and a capacitance (C). In the present work, for each semi-circular curve on a complex impedance diagram (Fig. 3) that characterizes the bulk conduction mechanism of a sample that occurs in the frequency range of 10^3–10^6 Hz, the relationship between all of the aforementioned parameters for each complex impedance spectrum can be described as follows:

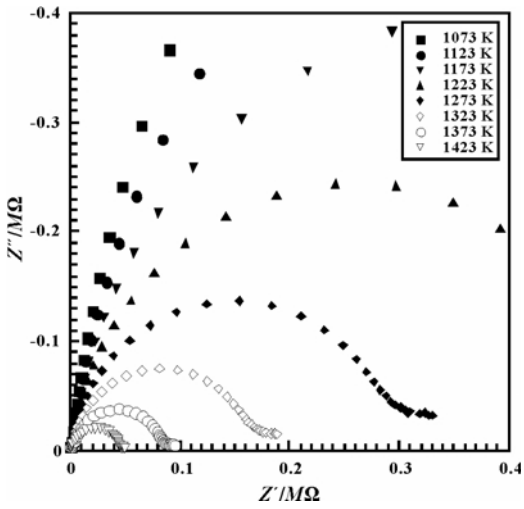

FIG. 3. Nyquist diagram of the real and imaginary components of the dry polycrystalline olivine compacts under conditions of P = 4.0 GPa, T = 1073–1423 K, and oxygen fugacity controlled by means of a Mo-MoO_2 solid buffer. The experimental frequencies increase from right to left along each semi-circle of the impedance spectra.

$$Z^* = Z' - \mathrm{j}Z'' = |Z|\cos\Phi - |Z|\sin\Phi = \frac{R - \mathrm{j}\omega CR^2}{1 + \omega^2 C^2 R^2} \quad (3)$$

where $\omega = 2\pi f$ is the angular frequency, f is the frequency, * represents a complex quantity, and j is $\sqrt{-1}$.

Under controlled pressure, temperature and oxygen fugacity, we ran *ZPlot* software in a Solartron-1260 impedance/gain-phase analyzer

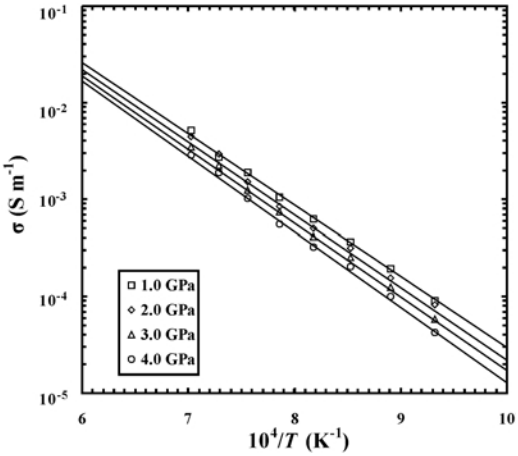

FIG. 4. Electrical conductivity *vs.* the inverse temperature for the dry polycrystalline olivine compacts under the conditions of P = 1.0–4.0 GPa, T = 1073–1423 K, and oxygen fugacity controlled by means of a Mo-MoO_2 solid buffer.

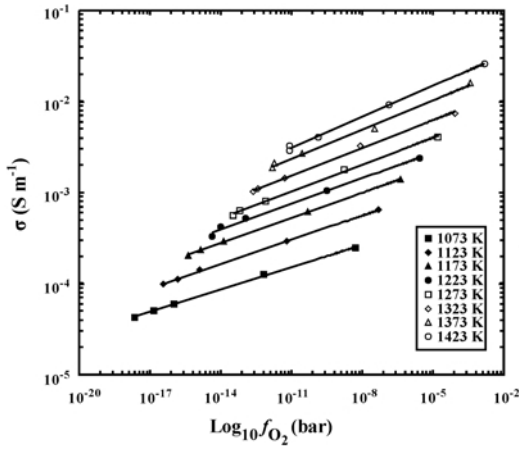

FIG. 5. Relationship between electrical conductivity and oxygen fugacity for dry polycrystalline olivine compacts under conditions of P = 4.0 GPa, eight temperatures between 1073 and 1423 K and for the five metal-oxygen buffers: Fe_3O_4-Fe_2O_3, Ni-NiO, Fe-Fe_3O_4, Fe-FeO and Mo-MoO_2.

and automatically registered the complex impedance spectra of the synthetic polycrystalline olivine compacts (Ohta *et al*., 2008). The *ZView* program is adapted to fit these data and obtain the impedance value of the samples measured (Ohta *et al*., 2010*b*). Using equation 4, therefore, the electrical conductivities of the sample can be calculated:

$$\sigma = \frac{1}{\pi \times r^2 \times R} \quad (4)$$

where σ is the electrical conductivity of the sample (S/m), l is the length of the recovery sample (m), r is the electrode diameter of the recovery sample (m), and R is the resistance (Ω).

Under specific pressure and oxygen fugacity conditions, the relationship between the logarithm of the sample's electrical conductivity and the reciprocal of the temperature satisfy the Arrhenius equation:

$$\log_{10}\sigma = \log_{10}\sigma_0 \times \log_{10} e \times \left(-\frac{\Delta H}{RT}\right) \quad (5)$$

where σ is the electrical conductivity of the sample (S/m), σ_0 is the pre-exponential factor that is independent of temperature (S/m), ΔH is the activation enthalpy (kJ/mol), and R is the ideal gas constant (kJ/mol/K). The relationship between the activation enthalpy and the activation energy can be described as follows:

$$\Delta H = \Delta U + P \times \Delta V \quad (6)$$

where ΔH is the activation enthalpy (kJ/mol), ΔU is the activation energy (kJ/mol), P is pressure (kPa), and ΔV is the activation volume (cm^3/mol).

TABLE 2. Arrhenius-fitted parameters of the electrical conductivity of polycrystalline olivine compacts using a Mo-MoO_2 oxygen buffer.

P (GPa)	T (Kelvin)	Log σ_0	ΔH (eV)	σ_0 (S/m)	r^2
1.0	1073–1423	2.9073±0.1152	143.7710±2.7358	807.8486±1.3038	0.9977
2.0	1073–1423	2.9334±0.1720	145.9496±2.0427	857.8276±1.4860	0.9953
3.0	1073–1423	2.9277±0.0976	148.1861±2.3175	846.6424±1.2519	0.9985
4.0	1073–1423	2.9647±0.1301	151.4444±3.0906	921.9344±1.3493	0.9976

The results are given in Figs 4 and 5 and Table 2. Figure 4 describes the functional relationship between the electrical conductivity of dry polycrystalline olivine compacts and the inverse of the temperature under the conditions of P = 1.0–4.0 GPa, T = 1073–1423 K, and an oxygen fugacity controlled by Mo-MoO_2. Figure 5 describes the relationship between the electrical conductivity of the sample and oxygen fugacity under P = 4.0 GPa, T = 1073–1423 K, and an oxygen fugacity controlled by the aforementioned five solid buffers. Table 2 describes the Arrhenius-fitted parameters of the electrical conductivity of the sample.

Summary and Discussion

In the present experiment, by controlling the conditions such as frequency, temperature, pressure and oxygen fugacity, we successfully obtained a series of data concerning the electrical conductivity of dry polycrystalline olivine compacts. The electrical conductivities of the samples under non-ambient conditions (Fig. 4, Table 2) reveal the strong linear dependence of electrical conductivity on temperature, and, moreover, that the correlated linear coefficient is even greater ($r^2 \geqslant 0.9953$). As a function of increasing pressure, the electrical conductivities of the samples decrease, whereas the activation enthalpy and temperature-independent pre-exponential factors increase slightly. The results of the present study are similar to previous studies of the electrical conductivities of dry samples such as single-crystal olivine, single-crystal pyroxene, and pyrope-rich garnet in the upper mantle (Xu *et al*., 1998, 2000*b*; Dai *et al*., 2006, 2009*c*). Furthermore, given the results of activation enthalpy, we can calculate the activation energy and activation volume of the samples, which are 141.02±2.53 kJ/mol and 0.25±0.05 cm^3/mol, respectively. These values are very close to those observed (by Xu *et al*., 1998, 2000*b*, ΔH = 154 kJ/mol and ΔV = 0.09 to ~0.68 cm^3/mol) for dry polycrystalline San Carlos olivine under conditions of 4–10 GPa, 1273–1673 K and a Mo-MoO_2 solid buffer.

Figure 5 depicts the functional relationship between the electrical conductivity of the sample and oxygen fugacity under conditions of 4.0 GPa, 1073–1423 K, and five different solid buffers. The buffers are more oxidizing in the order: Mo-MoO_2, Fe-FeO, Fe-Fe_3O_4, Ni-NiO and Fe_3O_4-Fe_2O_3 and the electrical conductivity of the sample increases with increasing oxygen fugacity. These results define a theoretical model that describes the relationship between electrical conductivity and oxygen fugacity for dry polycrystalline olivine:

$$\log_{10}(\sigma) = (2.47 \pm 0.085) + (0.096 \pm 0.023) \times \log_{10} f_{O_2} + \frac{(-0.55 \pm 0.011)}{T} \quad (7)$$

According to Dai and Karato (2009*b*), the impact of oxygen fugacity on the electrical conductivity of dry wadsleyite can be elucidated by changing the charge-carrier concentration of the lattice defect. This effect is described by the Nernst-Einstein equation, which shows that the electrical conductivity of any substance is exactly equal to the total contributions by various conduction mechanisms (Xu and McCammon, 2002; Huang *et al*., 2005; Wu *et al*., 2010):

$$\sigma = \sum_i n_i q_i \mu_i \quad (9)$$

where σ is the electrical conductivity of the sample, n_i is the concentration of n-type charge carriers, q_i is the effective charge, and μ_i is the charge mobility. The defect chemistry of polycrystalline olivine compacts demonstrates that the concentration of the ferric-related defects $[X]$ relies on the chemical environment as follows:

$$[X] \propto f_{H_2O}^{p} f_{O_2}^{q} a_{MO}^{r} \quad (9)$$

where f_{H_2O} is the water fugacity, f_{O_2} is the oxygen fugacity, a_{MO} is the activity of MgO or FeO, and p, q and r are constants that depend on different defect types. According to the defect model of ferromagnesian silicate proposed by Karato (2008*b*), by using the positive dependence of electrical conductivity on oxygen fugacity in this experiment, we can describe the dependence of defect concentration in olivine for various charge-neutrality conditions on the chemical environment as:

$$[Fe_{Mg}^{\bullet}] = 2[V_{Mg}^{''}] \ (p = 0, q = 1/6, r = -1/3) \quad (10)$$

or

$$[Fe_{Mg}^{\bullet}] = [H_{Mg}^{'}] \ (p = 1/4, q = 1/8, r = -1/2) \quad (11)$$

where $Fe_{Mg}^{\bullet}$ is the ferric ion of the crystal lattice in the Mg site, $V_{Mg}^{''}$ are two vacancies in the Mg site, and H_{Mg} is the vacancy of a hydrogen proton in the crystal lattice of Mg site.

The activation enthalpy values of 143–151 kJ/mol for polycrystalline olivine compacts

are similar to experimental results that have been reported previously for dry single-crystal olivine (Xu *et al*., 1998, 2000*b*) and pyrope-rich garnet (Dai and Karato, 2009*c*). There is strong evidence of a small polaron conduction mechanism, i.e. $Fe^{\bullet}_{Mg}$ is the ferric ion of the crystal lattice in the Mg site, based on the dependence of electrical conductivity on oxygen fugacity. The small polaron conduction sample is thermally activated, such that holes hop from ferric to ferrous Fe in the Mg lattice sites. The exponential value q (~0.096), which describes the variation of electrical conductivity in the sample and oxygen fugacity, is less than estimated by Models 10 and 11 at room pressure (Wanamaker and Duba, 1993; Hirsch *et al.*, 1993; Du Frane *et al*., 2005; Karato, 2008*b*; Farla *et al*., 2010). This may be due to other electrical neutrality conditions which are independent of oxygen fugacity, such as $Fe^{\bullet}_{Mg} = [e']$, which is also involved in the process of electrical conduction.

Conclusion

By varying the type of solid buffer to control oxygen fugacity in the YJ-3000t large-volume, multianvil press, we successfully conducted *in situ* measurements of the electrical conductivities of polycrystalline olivine compacts. When there is no existing evidence that can be used to determine the conduction mechanism of the thermoelectric coefficient, oxygen fugacity is thought to be the most efficient and straightforward method for identifying the conduction mechanism of minerals and rocks at high temperatures and pressures.

Acknowledgements

The authors are grateful to S. Karato of the Department of Geology and Geophysics at Yale University for helpful discussions during the preparation of the manuscript. M. Mookherjee of Bayreuth Geoinsitut helped to complete the FTIR measurement. Z.T. Jiang and Z.C. Jing of Yale University provided technical assistance with collection of Raman spectra. Professor M.Z. Wang of the Institute of Geochemistry of the Chinese Academy of Sciences performed the EPMA analysis on the samples. We are grateful to 'American Journal Experts' for their help with improving the English in the manuscript. This research is supported financially by the Knowledge-Innovation Key Orientation Project of CAS (Grant Nos. KZCX2-YW-Q08-3-4, KZCX2-YW-QN110 and KZCX3-SW-124), the Large-scale Scientific Apparatus Development Program of the CAS (Grant No. YZ200720), the 863 High Technology Research and Development Program of China (Grant No. 2006AA09Z205), and the NSF of China (Grant Nos. 40974051, 40704010 and 40573046).

References

Bagdassarov, J.M.N. and Schmeling, H. (2005) Electrical conductivity and partial melting of mafic rocks under pressure. *Geochimica et Cosmochimica Acta*, **69**, 4703–4718.

Campbell, A.J., Danielson, L., Righter, K., Seagle, C.T., Wang, Y. and Prakapenka, V.B. (2009) High pressure effects on the iron–iron oxide and nickel–nickel oxide oxygen fugacity buffers. *Earth and Planetary Science Letters*, **286**, 556–564.

Chou, I.M. (1978) Calibration of oxygen buffers at elevated P and T using the hydrogen fugacity sensor. *American Mineralogist*, **63**, 690–703.

Chou, I.M. and Eugster, H.P. (1976) Fugacity control and dissociation constants of HBr and HI. *Contributions to Mineralogy and Petrology*, **56**, 77–100.

Dai, L., Li, H., Liu, C., Su, G. and Shan, S. (2006) Experimental measurements of the electrical conductivity of pyroxenite at high temperature and high pressure under different oxygen fugacities. *High Pressure Research*, **26**, 193–202.

Dai, L., Li, H., Deng, H., Liu, C., Su, G., Shan, S., Zhang, L. and Wang, R. (2008*b*) *In situ* control of different oxygen fugacity experimental study on the electrical conductivity of lherzolite at high temperature and high pressure. *Journal of Physics and Chemistry of Solids*, **69**, 101–110.

Dai, L., Li, H., Hu, H. and Shan, S. (2009*a*) Novel technique to control oxygen fugacity during high-pressure measurements of grain boundary conductivities of rocks. *Review of Scientific Instruments*, **80**, 033903, doi: 10.1063/1.3097882.

Dai, L. and Karato, S. (2009*b*) Electrical conductivity of wadsleyite at high temperatures and high pressures. *Earth and Planetary Science Letters*, **287**, 277–283.

Dai, L. and Karato, S. (2009*c*) Electrical conductivity of pyrope-rich garnet at high temperature and high pressure. *Physics of the Earth and Planetary Interiors*, **176**, 83–88.

Dai, L. and Karato, S. (2009*d*) Electrical conductivity of orthopyroxene: Implications for the water content of the asthenosphere. *Proceedings of the Japanese Academy (series B)*, **85**, 466–475.

Dobson, D.P. and Brodholt, J.P. (1999) The pressure medium as a solid-state oxygen buffer. *Geophysical Research Letters*, **26**, 259–262.

Du Frane, W.L., Roberts, J.J., Toffelmier, D.A. and Tyburczy, J.A. (2005) Anisotropy of electrical conductivity in dry olivine. *Geophysical Research Letters*, **32**, L24315, doi: 10.1029/2005GL023879.

Farla, R.J.M., Peach, C.J. and ten Grotenhuis, S.M. (2010) Electrical conductivity of synthetic iron-bearing olivine. *Physics and Chemistry of Minerals*, **37**, 167–178.

Frost, B.R. (1991) Introduction to oxygen fugacity and its petrologic importance. Pp. 1–9 in: *Oxide Minerals: Petrologic and Magnetic Significance* (P.H. Lindsey, editor). Reviews in Mineralogy, **25**, Mineralogical Society of America, Washington, D.C.

Hirsch, L.M., Shankland, T.J. and Duba, A.G. (1993) Electrical conduction and polaron mobility in Fe-bearing olivine. *Geophysical Journal International*, **114**, 36–44.

Huang, X.G., Xu, Y.S. and Karato, S. (2005) Water content of the mantle transition zone from the electrical conductivity of wadsleyite and ringwoodite. *Nature*, **434**, 746–749.

Irifune, T. and Ringwood, A.E. (1987) Phase transformations in primitive MORB and pyrolite compositions to 25 GPa and some geophysical implications. Pp. 231–242 in: *High-Pressure Research in Mineral Physics* (M.H. Manghnani and Y. Syono, editors). Terra Scientific Publishing Company, Tokyo/ American Geophysical Union, Washington, D.C.

Karato, S. (2008*a*) Recent progress in the experimental studies on the kinetic properties in minerals. *Physics of the Earth and Planetary Interiors*, **170**, 152–155.

Karato, S. (2008*b*) *Deformation of Earth Materials: Introduction to the Rheology of the Solid Earth*, Cambridge University Press, Cambridge, UK, 463 pp.

Karato, S. and Dai, L. (2009) Comments on "Electrical conductivity of wadsleyite as a function of temperature and water content" by Manthilake et al. *Physics of the Earth and Planetary Interiors*, **174**, 19–21.

Li, H., Xie, H., Guo, J., Zhang, Y., Xu, Z. and Xu, J. (1998) In situ control of oxygen fugacity at high temperature and high pressure: A Ni-O system. *Geophysical Research Letters*, **25**, 817–820.

Li, H., Xie, H., Guo, J., Zhang, Y. and Xu, Z. (1999) In situ control of oxygen fugacity at high temperature and high pressure. *Journal of Geophysical Research*, **104**, 29439–29451.

McCammon, C.A., Frost, D.J., Smyth, J.R., Laustsen, H.M.S., Kawamoto, T., Ross, N.L. and Aken, P.A. (2004) Oxidation state of iron in hydrous mantle phases: Implications for subduction and mantle oxygen fugacity. *Physics of the Earth and Planetary Interiors*, **143–144**, 157–169.

Mendybaev, R.A., Beckett, J.R., Stolper, E. and Grossman, L. (1998) Measurement of oxygen fugacities under reducing conditions: Non-Nernstian behavior of Y_2O_3-doped zirconia oxygen sensors. *Geochimica et Cosmochimica Acta*, **62**, 3131–3139.

Nishihara, Y., Shinmei, T. and Karato, S. (2006) Grain-growth kinetics in wadsleyite: Effects of chemical environment. *Physics of the Earth and Planetary Interiors*, **154**, 30–43.

Nishihara, Y., Shinmei, T. and Karato, S. (2008) Effect of chemical environment on the hydrogen-related defect chemistry in wadsleyite. *American Mineralogist*, **93**, 831–843.

Nover, G. (2005) Electrical properties of crustal and mantle rocks – A review of laboratory measurements and their explanation. *Survey in Geophysics*, **26**, 593–651.

Ohta, K., Onoda, S., Hirose, K., Sinmyo, R., Shimizu, K., Sata, N., Ohishi, Y. and Yasuhara, A. (2008) The electrical conductivity of post-perovskite in Earth's D″ layer. *Science*, **320**, 89–91.

Ohta, K., Hirose, K., Ichiki, M., Shimizu, K., Sata, N. and Ohishi, Y. (2010*a*) Electrical conductivities of pyrolitic mantle and MORB materials up to the lowermost mantle conditions. *Earth and Planetary Science Letters*, **289**, 497–502.

Ohta, K., Hirose, K., Shimizu, K., Sata, N. and Ohishi, Y. (2010*b*) The electrical resistance measurements of $(Mg,Fe)SiO_3$ perovskite at high pressures and implications for electronic spin transition of iron. *Physics of the Earth and Planetary Interiors*, **180**, 154–158.

Omura, K., Kurita, K. and Kumazawa, M. (1989) Experimental study of pressure dependence of electrical conductivity of olivine at high temperatures. *Physics of the Earth and Planetary Interiors*, **57**, 291–303.

Ringwood, A.E. (1975) *Composition and Petrology of the Earth's Mantle*. McGraw Hill, New York, pp. 231–249.

Ringwood, A.E. (1982) Phase transformations and differentiation in subducted lithosphere: implications for mantle dynamics, basalt petrogenesis and crustal evolution. *Journal of Geology*, **90**, 611–643.

Roberts, J.J. and Duba, A.G. (1995) Transient electrical response of San Quintin dunite as a function of oxygen fugacity changes: Information about charge carriers. *Geophysical Research Letters*, **22**, 453–456.

Romano, C., Poe, B.T., Kreidie, N. and McCammon, A. (2006) Electrical conductivities of pyrope-almandine garnets up to 19 GPa and 1700ºC. *American Mineralogist*, **91**, 1371–1377.

Romano, C., Poe, B.T., Tyburczy, J. and Nestola, F. (2009) Electrical conductivity of hydrous wadsleyite. *European Journal of Mineralogy*, **21**, 615–622.

Rubie, D.C., Karato, S., Yan, H. and O'Neill, H.St.C.

(1993) Low differential controlled chemical environment in multianvil high-pressure experiments. *Physics and Chemistry of Minerals*, **20**, 315–322.

Tyburczy, J.A. and Roberts, J.J. (1990) Low frequency electrical response of polycrystalline olivine compacts: Grain boundary transport. *Geophysical Research Letters*, **17**, 1985–1988.

Wanamaker, B.J. and Duba, A.G. (1993) Electrical conductivity of San Carlos olivine along [100] under oxygen-and pyroxene-buffered conditions and implications for defect equilibria. *Journal of Geophysical Research*, **98**, 489–500.

Wang, D., Mookherjee, M., Xu, Y.S. and Karato, S. (2006) The effect of water on the electrical conductivity of olivine. *Nature*, **443**, 977–980.

Watson, H.C., Roberts, J.J. and Tyburczy, J.A. (2010) Effect of conductive impurities on electrical conductivity in polycrystalline olivine. *Geophysical Research Letters*, **37**, L02302, doi: 10.1029/2009GL041566.

Weston, L.R., Brenan, J.A., Fei, Y.W., Secco, R.A. and Frost, D.J. (2009) Effect of pressure, temperature, and oxygen fugacity on the metal-silicate partitioning of Te, Se, and S: Implications for earth differentiation. *Geochimica et Cosmochimica Acta*, **73**, 4598–4615.

Wu, X.P., Zhang, B.H., Xu, J.S., Katsura, T., Zhai, S.M., Yoshino, T., Manthilake, G. and Shatskiy, A. (2010) Electrical conductivity measurements of periclase under high pressure and high temperature. *Physica B*, **405**, 53–56.

Xie, H.S., Zhou, W.G., Zhu, M.X., Liu, Y.G., Zhao, Z.D. and Guo, J. (2002) Elastic and electrical properties of serpentinite dehydration at high temperature and high pressure. *Journal of Physics: Condensed Matter*, **14**, 11359–11363.

Xu, Y.S. and McCammon, C. (2002) Evidence for ionic conductivity in lower mantle $(Mg,Fe)(Si,Al)O_3$ perovskite. *Journal of Geophysical Research*, **107**, B102251, doi: 10.1029/2001JB000677.

Xu, Y.S., Poe, B.T., Shankland, T.J. and Rubie, D.C. (1998) Electrical conductivity of olivine, wadsleyite, and ringwoodite under upper-mantle conditions. *Science*, **280**, 1415–1418.

Xu, Y.S., Shankland, T.J. and Poe, B.T. (2000*a*) Laboratory-based electrical conductivity in the earth's mantle. *Journal of Geophysical Research*, **105**, 27865–27875.

Xu, Y.S., Shankland, T.J. and Duba A.G. (2000*b*) Pressure effect on electrical conductivity of mantle olivine. *Physics of the Earth and Planetary Interiors*, **118**, 149–161.

Yasuda, A. and Fujii, T. (1993) Application of a solid-electrolyte oxygen fugacity sensor to high-pressure experiments. *Physics of the Earth and Planetary Interiors*, **80**, 49–64.

Zhang, B.H., Katsura, T., Shatskiy, A., Matsuzaki, T. and Wu, X.P. (2006) Electrical conductivity of $FeTiO_3$ ilmenite at high temperature and high pressure. *Physical Review*, **B73**, 134104, doi: 10.1103/PhysRevB.73.134104.

Zhang, B.H., Wu, X.P., Xu, J.S., Katsura, T. and Yoshino, T. (2010) Electrical conductivity of enstatite up to 20 GPa and 1600 K. *Chinese Journal of Geophysics*, **53**, 760–764.